# Nanoscale Networked Single-Walled Carbon-Nanotube Electrodes for Transparent Flexible Nanogenerators

**Dukhyun Choi,[†] Min-Yeol Choi,[‡] Hyeon-Jin Shin,[†] Seon-Mi Yoon,[†] Ju-Seok Seo,[‡] Jae-Young Choi,*[,†] Sang Yoon Lee,[†] Jong Min Kim,[†] and Sang-Woo Kim*[,§]**

*Samsung Advanced Institute of Technology, Yongin, Gyeonggi 446-712, Republic of Korea, School of Advanced Materials and System Engineering, Kumoh National Institute of Technology, Gumi, Gyeongbuk 730-701, Republic of Korea, School of Advanced Materials Science and Engineering, Center for Human Interface Nanotechnology (HINT), SKKU Advanced Institute of Nanotechnology (SAINT), Sungkyunkwan University, Suwon 440-746, Republic of Korea*

*Received: October 10, 2009; Revised Manuscript Received: November 24, 2009*

We have investigated a nanoscale networked single-walled carbon-nanotube (SWCNT) electrode as a top cathode electrode of transparent flexible (TF) nanogenerators, so as to improve the energy scavenging performance and the system stability. The morphological effect and the electrical stability of SWCNT films for TF nanogenerators are investigated. It is found that SWCNT films have a nanosized network surface with pores, exceeding 100 nm in size, which favor ZnO nanorods contacting the CNT electrode, increasing the current generation and reducing the series resistance of the device for the effective transportation of piezoelectrically generated electrons from the nanogenerators. The nanogenerator using the CNT electrode with transparency 84% (at wavelength 550 nm) and a sheet resistance of 220 Ω/square had approximately 5 times the current density as with an indium−tin oxide-based nanogenerator. Moreover, the low variation (<100 Ω) in the resistance of CNT films during bending tests, and small change of the resistance of the film before and after the bending test (less than 1.1% on average), can support durable, stable, and reliable CNT-based TF nanogenerators.

## 1. Introduction

Carbon nanotubes (CNTs) are acknowledged as promising building blocks in diverse applications, from high strength materials to artificial muscles and nanoelectronics, as a result of their unusual geometric, electric, thermal, optical, and mechanical properties.[1−4] As examples, CNT-based transistors,[5] biosensors,[6] lithium-ion batteries,[7,8] and optoelectronic devices[9,10] have been developed with exceptional performance. On the basis of their high conductivity, transparency, and mechanical stability, an application with rapidly increasing commercial demand is as a transparent electrode material for flexible organic electronics, such as organic light-emitting diodes and organic photovoltaics.[11−14] To date, indium tin oxide (ITO) films have mainly been used as transparent flexible (TF) electrodes in electronic devices but ITO has limited flexibility due to its ceramic structure, and defects can be introduced if it is overflexed.[13−15] CNT network sheets are now being considered as a new TF electrode with alternate ITO electrodes.

A self-powered nanogenerator based on a piezoelectric zinc oxide (ZnO) nanowire was developed in 2006, triggering an explosion of studies in such applications as piezoelectric field-effect transistors, force/pressure sensors, and resonators.[16−18] The great advantage of the ZnO nanowire-based nanogenerator is that rectifying current and potential can be generated due to the coupled piezoelectric and semiconducting properties of ZnO[19,20] by a variety of external stimulations, such as body movement (pushing, bending, and stretching), vibrations (heart beat, noise, acoustic and ultrasonic waves), and hydraulic or air forces (blood and wind flow).[21−23] The previous work has demonstrated that TF nanogenerators with piezoelectric ZnO nanorods can be driven by direct pushing or bending of the TF nanogenerator itself.[23] The effects of surface morphology and Schottky contact for a generated current output and efficiency have also been characterized, demonstrating that a cathode electrode with a rugged surface and a high work function is highly effective. However, the mechanical durability of the ITO electrodes used in the fully TF nanogenerators is inadequate for lifetime and electrical/mechanical stability, and the monotonously flat surface acting as the top electrode leads to low contact probability (i.e., small number of active nanorods and high series resistance) between ZnO nanorods and the top electrode during pushing or bending, thereby reducing the output current density.

Here, we report a single-walled CNT (SWCNT) network sheet as the top cathode electrode of TF nanogenerators so as to improve the energy scavenging performance and the system stability. The morphological effect and the electrical stability of CNT films for TF nanogenerators are investigated. It is found that CNT films have a nanosized network surface with pores, exceeding 100 nm in size, which favor ZnO nanorods contacting the CNT electrode, increasing the current generation, and reducing the series resistance of the device for the effective transportation of piezoelectrically generated electrons from the nanorods. The nanogenerator using the CNT electrode with transparency 84% (at wavelength 550 nm) and a sheet resistance of 220 Ω/square had approximately 5 times the current density as with an ITO-based nanogenerator. Moreover, the low variation (<100 Ω) in the resistance of CNT films during bending tests, and small change of the resistance of the film

* To whom correspondence should be addressed. E-mail:kimsw1@skku.edu (S.-W.K.), jaeyoung88.choi@samsung.com (J.-Y.C.).
[†] Samsung Advanced Institute of Technology.
[‡] Kumoh National Institute of Technology.
[§] Sungkyunkwan University.

10.1021/jp909713c 
Published on Web 12/16/2009

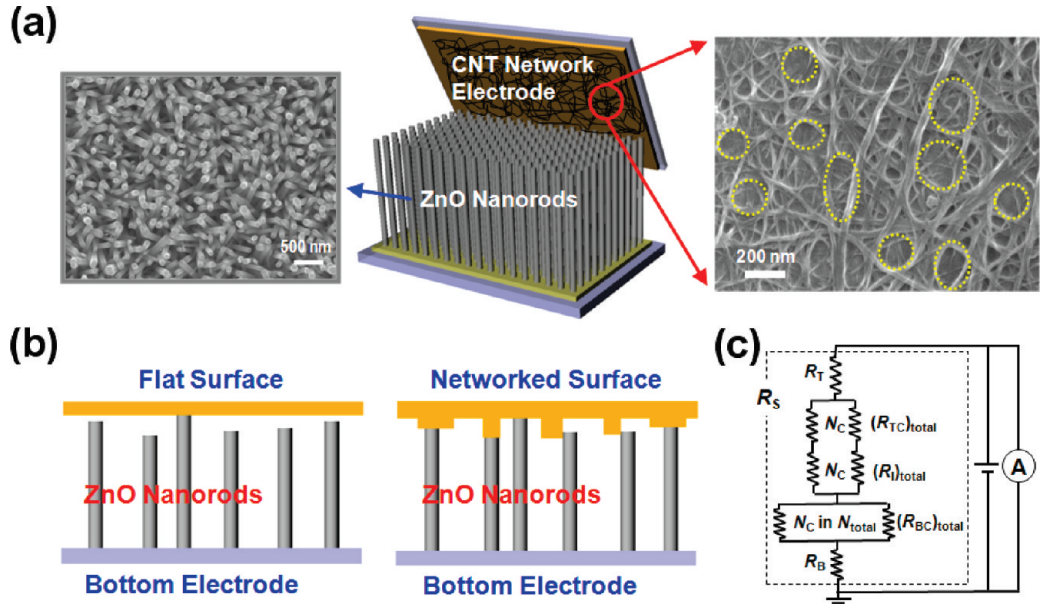


**Figure 1.** CNT-based TF nanogenerator. (a) Schematic illustration of an integrated TF nanogenerator (middle). FE-SEM images of ZnO nanorods grown on an ITO/PES substrate (left) and a SWCNT network sheet on a PEN substrate (right). (b) Schematic cross-section of nanogenerators; a top electrode with a flat surface (left) and a top electrode with a networked surface at nanoscale (right). (c) Equivalent circuit of a nanogenerator. $N_{total}$ indicates the total number of grown ZnO nanorods, whereas $N_C$ is the number of ZnO nanorods forming a contact with the top electrode.

before and after the bending test (less than 1.1% on average), can support durable, stable, and reliable CNT-based TF nanogenerators.

## 2. Experimental Section

We used highly purified arc discharge SWCNTs with a mean diameter of 1.4 nm and purity of 93 wt % (Iljin Nanotech Co., Ltd.). SWCNTs (15 mg) were dispersed with 30 mg of sodium dodecylbenzene sulfonate (NaDDBS) in deionized (DI) water (30 mL) and were sonicated by a bath type sonicator (RK 106, Bandelin Electronic, Berlin, Germany) for 10 h at 240 W. After ultrasonication the samples were immediately precipitated in a centrifuge (4239R-V4, ALC International Srl, Italy) at 8000 rpm for 10 min, so as to eliminate the bundled SWCNTs in the SWCNT solution. By using a specific volume of the supernatant of the SWCNT solution, CNT network electrodes were successfully fabricated on polyethylene naphthalate (PEN) substrates using spraying equipment (NVD-200, Fujimori, Japan). To improve conductance, CNT films were dipped in nitric acid solutions for 1 h and were then rinsed several times in DI water.[24,25] ZnO nanorods were synthesized on ITO-coated polyethersulfone (PES) substrates using the aqueous solution method.[23] As a seed solution, we used zinc acetate dehydrate [$Zn(CH_3COO)_2 \cdot 2H_2O$, 0.01 M] dissolved in ethanol (100 mL) that had been heated at 90 °C. The seed solution was spin-coated at 5000 rpm for 20 s. The seed coated substrate was dried onto a hot template at 100 °C for 10 min. After 6 times of spin-coating and the annealing, ZnO nanorods were formed in aqueous solution, using zinc nitrate hexahydrate [$Zn(NO_3)_2 \cdot 6H_2O$, 0.025 M], hexamethylenetetramine (0.025 M), and DI water (250 mL). The main growth of the ZnO nanorods took place at 95 °C for 3 h.

Field-emission scanning electron microscopy (FE-SEM) was undertaken using a JEOL JSM 6500 instrument. Atomic force microscopy (AFM) images were taken using an AFM Dimension V (Veeco Co.) in a tapping mode. The scan speed was 1 Hz, and the scan size was 2 × 2 $\mu m^2$ for the detailed morphology and 10 × 10 $\mu m^2$ for the surface roughness. The surface roughness was determined as the average value from five different positions. Transmission spectra were obtained using a Varian Cary 5000 UV−vis spectrometer. The sheet resistance of the films was measured by a four-point probe method (ChangMin, LTD, CMT-SR2000N, Korea). Current−voltage (I−V) measurements to evaluate the formation of Schottky contacts between the ZnO nanorods and the top electrode, and the series resistance of the devices, were carried out using an Agilent 4156A parameter analyzer. A Keithley 6485 pico-ammeter was used for low noise current measurements to detect currents generated by the TF nanogenerators. The work function of a SWCNT network electrode was measured by ultraviolet photoemission spectroscopy (UPS, Gammadata VUV 5050) using a He II discharge lamp ($h\nu$ = 40.8 eV).

## 3. Results and Discussion

Part a of Figure 1 is a schematic illustration of an integrated TF nanogenerator with a CNT cathode electrode and piezoelectric ZnO nanorods grown on an ITO/PES substrate. We have prepared the CNT films by spraying solutions of SWCNT onto a PEN substrate. As the typical FE-SEM image of part a of Figure 1 shows, the CNT film has a nanosized network surface morphology, with large pores (dot circles) exceeding 100 nm. This networked surface morphology of a CNT film with large pores offers high contact probability between ZnO nanorods of diameter about 100 nm and the CNT top electrode under a pushing or bending mode. For example, in the case of a top electrode with a flat surface (left of part b of Figure 1), the number of ZnO nanorods contacting the top electrode could be low as a result of the variation in the length or the tilted direction of ZnO nanorods. On the other hand, many ZnO nanorods could be in contact with the networked top electrode at nanoscale (right of part b of Figure 1) because long nanorods can enter into the large pores in the top electrode and short nanorods can touch the protruded surface of the top electrode. Thus, when a CNT film is applied to the top cathode electrode of TF nanogenerators, we expect an increase in active ZnO nanorods (i.e., generating

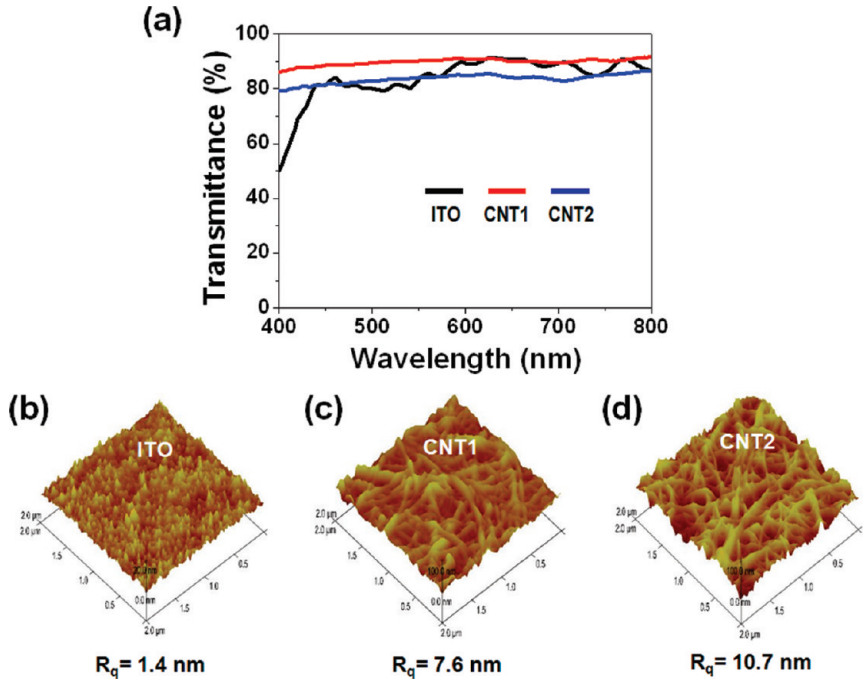


**Figure 2.** Optical and morphological characterizations of ITO and CNT films. (a) Transmittance of the films comparing the transparency of an ITO electrode on a PES substrate and CNT electrodes on PEN substrates (insert). (b) AFM images showing the surface morphology of the samples. Depending on the number of sprayings, the transmittance decreased from 91% (CNT1) to 84% (CNT2) at a wavelength 550 nm.

piezoelectric power) in contact with the top electrode, increasing the generating efficiency.

An equivalent electric circuit for the nanogenerators is shown in part c of Figure 1, so as to illustrate the contact conditions between the nanorods and the electrodes. The resistances of the bottom electrode, top electrode, and a single ZnO nanorod are respectively denoted by $R_B$, $R_T$, and $R_I$. The contact resistances between the nanorods and the electrodes are $R_{BC}$ (between the bottom electrode and the nanorods) and $R_{TC}$ (between the top electrode and the nanorods). We ignored the capacitance in the system and the contacts with external equipment to simplify the discussion. On the basis of the circuit diagram in part c of Figure 1, the series resistance ($R_S$) in this device, which is the total resistance of this system, is given by[26]

$$R_S = R_B + (R_{BC})_{total} + (R_I)_{total} + (R_{TC})_{total} + R_T = R_B + (R_{BC} + R_I + R_{TC})/N_C + R_T \quad (1)$$

where $N_C$ is the number of ZnO nanorods forming a contact with the top electrode when the top electrode is pushed by a human finger.[23] Because the nanorods bridging the top and the bottom electrode among all nanorods grown on the bottom electrode only contribute to the current output, other ZnO nanorods with no contact to the top electrode should be ruled out for estimating the $(R_{TC})_{total}$, $(R_{BC})_{total}$, and $(R_I)_{total}$. As shown in part b of Figure 1, $N_C$ is dependent on the surface morphology of the top electrode in a nanogenerator. According to the eq 1, $R_S$ is strongly dependent on $N_C$. Because a high $R_S$ causes great loss of current generated from ZnO nanorods, it is necessary to increase $N_C$ in nanogenerators to reduce the $R_S$ of the device.

In the previous work, we investigated the optimization of optical and electrical properties of CNT films by controlling the concentration of SWCNT solution, the spraying conditions, and the post-treatment.[24,27,28] Here, we first demonstrate the effect of morphology of the CNT film for TF nanogenerators. Part a of Figure 2 shows the transmittance of ITO film and CNT films with varying numbers of sprayings of a SWCNT solution. By controlling the number of sprayings, we obtained CNT

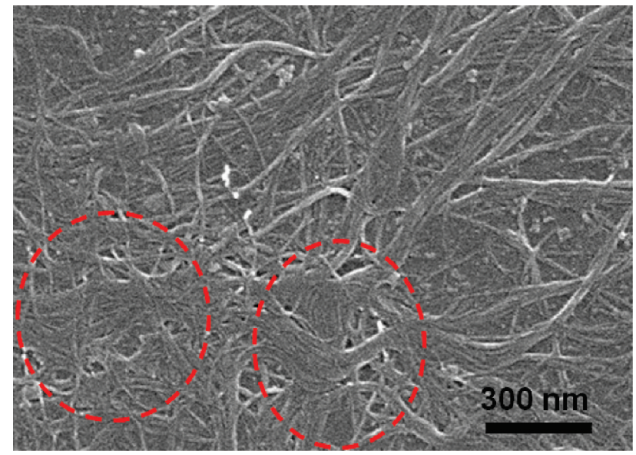


**Figure 3.** Bundling of SWCNTs by overspraying. Bundled SWCNTs on PEN after many spraying cycles of SWCNT solution. The pores (red dot circles) on the SWCNT network electrode were smaller than 100 nm or were clogged due to bundling of the SWCNTs.

electrode film (CNT1) with transparency exceeding 90%, which is greater than that of an ITO film (part a of Figure 2). As the number of spraying increases, the transparency of the CNT films falls. Parts b−d of Figure 2 show AFM images for ITO and CNT electrodes. A number of pores in the CNT surfaces larger than 100 nm are visible, but the surface of the ITO electrode on the PES substrate was fairly flat, without large pores (root-mean-square surface roughness, $R_q$ = 1.4 nm). In addition, as the number of sprayings increases from CNT1 to CNT2, the surface roughness increased from 7.6 to 10.7 nm, so that there should be more ZnO nanorods in contact with the CNT2 electrode than the CNT1 electrode. However, as the spraying increases further, we observed bundling of SWCNTs, so that the pore size decreased or clogging occurred as shown in Figure 3.

Part a of Figure 4 displays I−V curves for the nanogenerators based on ITO and CNT top electrodes. Although the sheet

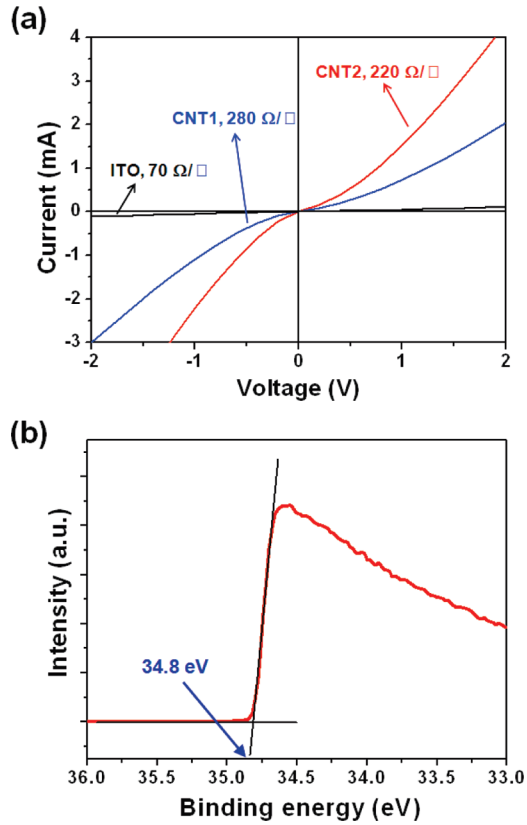


**Figure 4.** (a) I−V curves for ITO-, CNT1-, and CNT2-based nanogenerators. (b) The UPS spectrum measured for the work function of our SWCNT network electrode. The energy of the excitation photons ($h\nu$) during UPS measurements was 40.8 eV. On the basis of gold metal as a reference, the position of the Fermi level was calibrated by measuring the Fermi edge of the gold ($E_F = -1.13$ eV), the work function was estimated by $h\nu - (E_{cutoff} - E_F)$. Thus, the work function is determined to be 4.87 eV for our CNT films.

resistance of the ITO film (70 Ω/square) is lower than that of CNT1 film (280 Ω/ square), the current at 2 V in the I−V curve from the CNT1-based nanogenerator was 20 times greater than that from the ITO-based one (2 mA for the CNT1-based nanogenerators and 0.1 mA for the ITO-based nanogenerator), which were measured under a force (0.9 kgf)[23] originating from the slight push by a human finger. We attribute this greater current to the favorable surface morphology of the CNT film for nanogenerators. Because the number of ZnO nanorods ($N_2$) in contact with the CNT film increased, the $R_S$ of the CNT1-based nanogenerator was dramatically reduced, according to the eq 1, resulting in higher current for a given voltage. For the CNT2-based nanogenerator, the current in the I−V curve also doubled relative to the CNT1-based nanogenerator. We suggest that this high current is also due to the reduced $R_S$ in the CNT2-based nanogenerator as a result of the lower sheet resistance ($R_T = 220$ Ω/square) and the greater surface roughness ($R_q = 10.7$ nm) of the CNT2 film than the CNT1 film ($R_T = 280$ Ω/square and $R_q = 7.6$ nm).

In nanogenerators, the contact between a ZnO nanorod and a top cathode electrode should have a Schottky barrier so as to generate a cumulative current output, supposing that the electrons generated from ZnO nanorods flow to the top electrode. The electron affinity of ZnO is 4.35 eV[29] and the work function of an ITO electrode is 4.7 eV, so that ITO−ZnO contact forms a Schottky barrier even though the barrier is not high. In general, the work function of SWCNT electrodes is between 4.5 and 5 eV.[30,31] The work function of our CNT electrode was 4.87 eV according to the UPS result (part b of Figure 4). Thus, the Schottky barrier between a CNT electrode and a ZnO nanorod must be highly effective in accumulating piezoelectrically generated carriers at the CNT−ZnO interface. Generally, the Fermi level pinning effect by charge states at the interface is one of the most important factors for Schottky barrier formation regardless metal work function.[32] However, we ruled out the Fermi level pinning effect for the Schottky barrier formation because ZnO nanorod samples grown in the same synthesis condition were utilized for every nanogenerator in this work. The CNT-based devices display more Schottky-like characteristics in the I−V curve than the ITO-based device, which implies that CNT-based nanogenerators can provide effective direct-current power.

Figure 5 shows the in situ two-probe resistance of the ITO film and the CNT films for the bending test, showing the initial and maximum bending positions of the films. To release the high stress and strain at the gripping region of the films, we set up an initial position with an orientation angle of about 20° (upper picture in Figure 5). The sample was 5 cm long and 1.5 cm wide, and the radius of curvature ($r$) of the maximum bent film was 1 cm (lower picture in Figure 5). The bending rate was 1 Hz. The resulting change in resistance of CNT films before and after the bending test was on average 1.1% (0.9% for CNT1 and 1.3% for CNT2) over 90 s, and the variation in resistance during the test was less than 100 Ω. For an ITO film, the initial resistance was 283 Ω. After only one time bending test, the film was fractured and it was not recovered (left insert

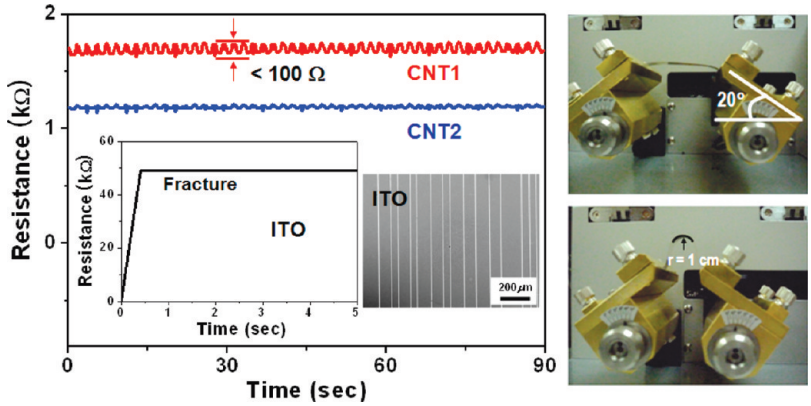


**Figure 5.** Electrical stability of CNT films in the bending test. The variation in the resistance of the CNT films and the ITO film during the bending test. An FE-SEM image of the ITO film after several bending tests. The pictures at right display the initial and the maximum positions of the films in the bending test.

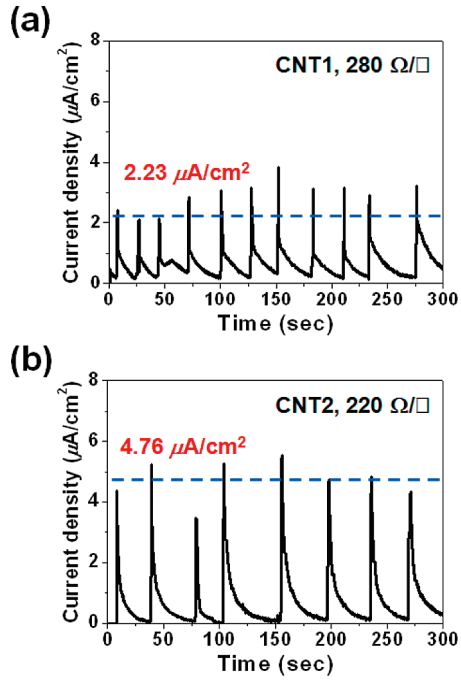


**Figure 6.** Output current density measured from TF nanogenerators. Current density generated from (a) the CNT1-based TF nanogenerator and (b) the CNT2-based TF nanogenerator.

in Figure 5). We found many cracks in the bent region of the ITO film (right insert in Figure 5). On the basis of our experimental bending results, we therefore assert that the CNT electrode film is suitable for making electrically and mechanically stable TF nanogenerators, especially those driven by pushing or bending of the device itself.

To investigate the effects of surface morphology and the electrical properties of the top electrode on the current scavenging performance of nanogenerators under the pushing mode, we prepared three different nanogenerators based on ITO, CNT1, and CNT2 top electrodes. The TF nanogenerator with the CNT1 top electrode gave an average current density of 2.23 $\mu$A/cm$^2$ at a load of 0.9 kgf. Although the sheet resistance of the CNT1 electrode (280 Ω/square) is greater than that of the ITO electrode (70 Ω/square), the output current density (part a of Figure 6) from the CNT1-based nanogenerator was about twice that from the ITO-based nanogenerator (data not shown, 0.9 $\mu$A/cm$^2$). The nanogenerator using CNT2 with a surface roughness of 10.7 nm and sheet resistance 220 Ω/square gave approximately five times the current density (4.76 $\mu$A/cm$^2$, part b of Figure 6) as the ITO-based nanogenerator. This is due to the improved contact between the ZnO nanorods and the top electrode using the SWCNT network electrode. We confirmed that the output currents originated from the piezoelectric charge generation rather than the instrument noise via switching-polarity tests.[22] It can be concluded that SWCNT network electrodes with surface morphology having pores larger than 100 nm are valuable in TF nanogenerators in increasing the number of active ZnO nanorods so as to enhance piezoelectric power generating events, and in reducing the $R_S$ of the system so as to reduce the generated current lost in the electrical transport process. The CNT top electrode is capable of producing high piezoelectric energy scavenging performance and high efficiency of the nanogenerators.

## 4. Conclusions

We have investigated a CNT top cathode electrode for TF nanogenerators for enhancing the output current density and system reliability. Because of the surface morphology, with large pores exceeding 100 nm, the CNT electrode led to an increase in the number of active ZnO nanorods contacting the top electrode under the pushing mode, resulting in more nanorods active in current generation and a decrease in the $R_S$ of the device, reducing the loss of transporting electrons. The SWCNT network electrode could have produced 4.76 $\mu$A/cm$^2$ from the CNT-based TF nanogenerator. Furthermore, the low variation (<100 Ω) in the resistance of CNT films during bending tests and small change (<1.1% on average) in the resistance of the film before and after the bending test promises durable, stable, and reliable CNT-based TF nanogenerators. The resulting effective and reliable CNT-based TF nanogenerators are capable of providing self-powered device applications or supplement energy sources such as self-powered chemical, biological, or haptic sensors, artificial robot skins, and battery supplements for cellular phones.

**Acknowledgment.** This research was supported by Basic Science Research Program through the National Research Foundation of Korea (NRF) funded by the Ministry of Education, Science and Technology (2009-0083540 and 2009-0077682).

## References and Notes

(1) Zhang, M.; Atkinson, K. R.; Baughman, R. H. *Science* **2004**, *306*, 1358–1361.
(2) Zhang, X. F.; Li, Q. W.; Tu, Y.; Li, Y. A.; Coulter, J. Y.; Zheng, L. X.; Zhao, Y. H.; Jia, Q. X.; Peterson, D. E.; Zhu, Y. T. *Small* **2007**, *3*, 244–248.
(3) Zhou, W.; Ren, L.; Lin, F.; Jiao, L.; Xue, T.; Xian, X.; Liu, Z. *Appl. Phys. Lett.* **2008**, *93*, 123115.
(4) Lee, E. J. H.; Balasubramanian, K.; Burghard, M.; Kern, K. *Adv. Mater.* **2009**, *21*, 2720–2724.
(5) Avouris, P.; Chen, Z. H.; Perebeinos, V. *Nat. Nanotechnol.* **2007**, *2*, 605–615.
(6) Minot, E. D.; Janssens, A. M.; Heller, I.; Heering, H. A.; Dekker, C.; Lemay, S. G. *Appl. Phys. Lett.* **2007**, *91*, 093507.
(7) Wen, Z. H.; Wang, Q.; Zhang, Q.; Li, J. H. *Adv. Funct. Mater.* **2007**, *17*, 2772–2778.
(8) Zhang, H.-X.; Feng, C.; Zhai, Y.-C.; Jiang, K.-L.; Li, Q.-Q.; Fan, S.-S. *Adv. Mater.* **2009**, *21*, 2299–2304.
(9) Vietmeyer, F.; Seger, B.; Kamat, P. V. *Adv. Mater.* **2007**, *19*, 2935–2940.
(10) Robel, I.; Bunker, B. A.; Kamat, P. V. *Adv. Mater.* **2005**, *17*, 2458–2463.
(11) Rowell, M. W.; Topinka, M. A.; McGehee, M. D.; Prall, H.-J.; Dennler, G.; Sariciftci, N. S.; Hu, L.; Gruner, G. *Appl. Phys. Lett.* **2006**, *88*, 233506.
(12) Tenent, R. C.; Barnes, T. M.; Bergeson, J. D.; Ferguson, A. J.; To, B.; Gedvilas, L. M.; Heben, M. J.; Blackburn, J. L. *Adv. Mater.* **2009**, *21*, 3210–3216.
(13) Willams, C. D.; Robles, R. O.; Zhang, M.; Li, S.; Baughman, R. H.; Zakhidov, A. A. *Appl. Phys. Lett.* **2008**, *93*, 183506.
(14) Rowell, M. W.; Topinka, M. A.; McGehee, M. D.; Prall, H. J.; Dennler, G.; Sariciftci, N. S.; Hu, L.; Gruner, G. *Appl. Phys. Lett.* **2006**, *88*, 233506.
(15) Parikh, J.; Saran, K.; Suh, D. S.; Muñoz, E.; Kolla, H.; Manohar, S. K. *J. Am. Chem. Soc.* **2004**, *126*, 4462–4463.
(16) Wang, X. D.; Song, J. H.; Liu, J.; Wang, Z. L. *Science* **2007**, *316*, 102–105.
(17) Wang, X. D.; Zhou, J.; Song, J. H.; Liu, J.; Xu, N. S.; Wang, Z. L. *Nano Lett.* **2006**, *6*, 2768–2772.
(18) Wang, Z. L. *Adv. Funct. Mater.* **2008**, *18*, 1–15.
(19) Green, L. E.; Law, M.; Yuhas, B. D.; Yang, P. *J. Phys. Chem. C* **2007**, *111*, 18451–18456.
(20) Mitrushchenkov, A.; Linguerri, R.; Chambaud, G. *J. Phys. Chem. C* **2009**, *113*, 6883–6886.
(21) Qin, Y.; Wang, X. D.; Wang, Z. L. *Nature* **2008**, *451*, 809–813.
(22) Yang, R.; Qin, Y.; Dai, L.; Wang, Z. L. *Nat. Nanotechnol.* **2009**, *4*, 34–39.

(23) Choi, M.-Y.; Choi, D.; Jin, M.-J.; Kim, I.; Kim, S.-H.; Choi, J.-Y.; Lee, S. Y.; Kim, J. M.; Kim, S.-W. *Adv. Mater.* **2009**, *21*, 2185–2189.

(24) Yoon, S.-M.; Kim, S. J.; Shin, H.-J.; Benayad, A.; Choi, S. J.; Kim, K. K.; Kim, S. M.; Park, Y. J.; Kim, G.; Choi, J.-Y.; Lee, Y. H. *J. Am. Chem. Soc.* **2008**, *130*, 2610–2616.

(25) Geng, H.-Z.; Kim, K. K.; So, K. P.; Lee, Y. S.; Chang, Y.; Lee, Y. H. *J. Am. Chem. Soc.* **2007**, *129*, 7758–7759.

(26) Because the ZnO nanorods are in parallel contact with the electrode, the contact resistance between the top electrode and the nanorods can be calculated by $(R_{TC})_{total} = R_{TC}/N$ when the top electrode is pushed by a human finger. 23 Similarly, the contact resistance between the bottom electrode and the nanorods can be determined by $(R_{BC})_{total} = R_{BC}/N$. Assuming that the individual active nanorods ($N$) have the same resistance by ignoring the variations of the dimensions in nanorods for simplicity, $(R_I)_{total}$ can be expressed by $R_I/N$.

(27) Shin, H.-J.; Kim, S. M.; Yoon, S.-M.; Benayad, A.; Kim, K. K.; Kim, S. J.; Park, H. K.; Choi, J.-Y.; Lee, Y. H. *J. Am. Chem. Soc.* **2008**, *130*, 2062–2066.

(28) Kim, K. K.; Bae, J. J.; Park, H. K.; Kim, S. M.; Geng, H.-Z.; Park, K. A.; Shin, H.-J.; Yoon, S.-M.; Benayad, A.; Choi, J.-Y.; Lee, Y. H. *J. Am. Chem. Soc.* **2008**, *130*, 12757–12761.

(29) Liu, Y. L.; Liu, Y. C.; Yang, H.; Wang, W. B.; Ma, J. G.; Zhang, J. Y.; Lu, Y. M.; Shen, D. Z.; Fan, X. W. *J. Phys. D* **2003**, *36*, 2705–2708.

(30) Pasquier, A. D.; Unalan, H. E.; Kanwal, A.; Miller, S.; Chhowalla, M. *Appl. Phys. Lett.* **2005**, *87*, 203511.

(31) Shiraishi, M.; Ata, M. *Carbon* **2001**, *39*, 1913–1917.

(32) Allen, M. W.; Durbin, S. M. *Appl. Phys. Lett.* **2008**, *92*, 122110.

JP909713C